JYX
JYVÄSKYLÄN YLIOPISTO
UNIVERSITY OF JYVÄSKYLÄ

This is a self-archived version of an original article. This version may differ from the original in pagination and typographic details.

Author(s): Annala, Leevi; Pölönen, Ilkka

Title: Kubelka-Munk Model and Stochastic Model Comparison in Skin Physical Parameter Retrieval

Year:

Version: Accepted version (Final draft)

Copyright: © The Authors, 2022

Rights: In Copyright

Rights url: http://rightsstatements.org/page/InC/1.0/?language=en

Please cite the original version:

Annala, L., & Pölönen, I. (2022). Kubelka-Munk Model and Stochastic Model Comparison in Skin Physical Parameter Retrieval. In T. T. Tuovinen, J. Periaux, & P. Neittaanmäki (Eds.), Computational Sciences and Artificial Intelligence in Industry : New digital technologies for solving future societal and economical challenges (pp. 137-151). Springer. Intelligent Systems, Control and Automation: Science and Engineering, 76. https://doi.org/10.1007/978-3-030-70787-3_10

Kubelka-Munk Model and Stochastic Model Comparison in Skin Physical Parameter Retrieval

Leevi Annala and Ilkka Pölönen

Abstract In medical field there is need for non-invasive diagnostic tools. One particular research area is skin cancer diagnostics. Here we study Kubelka-Munk model and stochastic skin reflectance model, which we combined from two sources to better reflect the physical structure of the skin. Our objective is to compare the models to each other in terms of accuracy, usefulness and biophysical parameter retrieval using convolutional neural network. The results are promising. Both model are found suitable options for further research and used stochastic model is similar to Kubelka-Munk in terms of accuracy. In physical parameter retrieval both models perform moderately. Inverted models reasonably retrieve the pigment concentrations from the simulated test data set. With empirical testing data the inverted models are mutually consistent.

1 Introduction

There is a need for automated non-invasive diagnostic methods for different illnesses and diseases in the medical field. Especially in case of melanomas and other skin cancers, the accuracy of the clinical diagnostic tools are poor, resulting in unnecessary operations and re-operations [9]. A well working non-invasive detection method could decrease the number of unnecessary operations and therefore bring savings to the hospital. One potential technology is combination of hyperspectral cameras, machine learning and neural networks in skin diagnostics [21, 23, 25].

Machine learning, and particularly training of the neural networks, require large amount of training data. A way to avoid laborious data gathering process is to use

Leevi Annala (✉)
University of Jyväskylä, e-mail: leevi.a.annala@jyu.fi

Ilkka Pölönen
University of Jyväskylä, e-mail: ilkka.polonen@jyu.fi

mathematical modelling in producing such augmented data set. Mathematical models for skin reflectance can be roughly divided into two categories: deterministic and stochastic [4]. Deterministic models are models where the inputs directly determine the output. Stochastic models include randomness. Examples of deterministic models include multitude of Kubelka-Munk equation based models [12, 26, 3, 6, 17, 1, 31, 7], Boltzmann photon transport equation [10], diffusion theory models [29] and many more, while stochastic modelling is exclusively based on Monte Carlo modelling [8, 27, 32, 19]. Model, that augments training data for machine learning, should have useful input parameters for inversion. This model should be easy to understand and modify and it should be sufficiently accurate.

Examples of previous research in non-invasive methods to determinate biochemical and biophysical skin properties using hyperspectral imaging include a study where skin thickness was successfully retrieved from hyperspectral image using inverted Kubelka-Munk Model [30]. The results were verified by ultrasound imaging and the machine learning method used in inversion was support vector regressor. Jolivot *et al.* retrieved melanin and blood concentrations and skin layer thicknesses from multispectral images [12]. They inverted Kubelka-Munk Model using genetic algorithm.

In this chapter we compare the Kubelka-Munk implementation of Jolivot *et al.* [12] to our own implementation of Stochastic Model, which is based on multilayered stochastic radiative transfer model by Maier *et al.* [19] and parameters described in [11]. Our objective is to use both models to skin reflectance modeling and compare them in terms of accuracy, usefulness and inversion with convolutional neural network [18]. Based on our knowledge this approach of stochastic modeling and convolutional neural network has not been used previously in skin physical parameter retrieval.

2 Materials and Methods

2.1 Stochastic Model

Stochastic Model (SM) is a Markov chain based model for the light propagation in layered media. The SM we use is modified from [19], by changing the pigments to those of the skin and using more general absorption and scattering coefficients. The basic principle of the SM is that the skin is seen as a network of states, and there is a certain probability of each transition between two states. The states and possible transitions are described in Figure 1. For this study, we assume that the skin has two layers: epidermis and dermis. Light that goes past these two layers is considered absorbed. The transition probabilities (P) are based on Beer's law and calculated as follows[19]. For up and down states the up/down, scattering and absorption probabilities are [19]

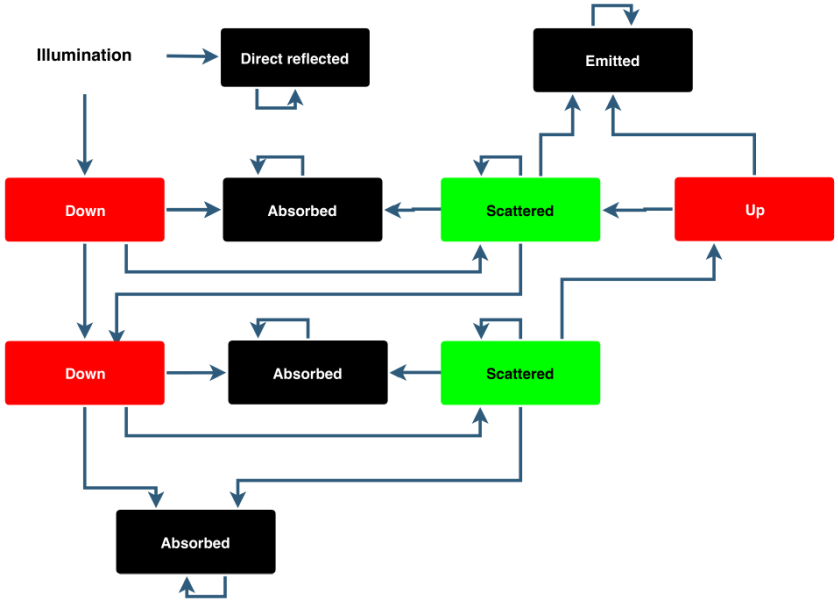

Fig. 1 Network of states and transitions in Stochastic Model.

$$P_{\text{up/down}}(\lambda) = 1 - P_{\text{absorption}} - P_{\text{scattering}}, \tag{1}$$

$$P_{\text{scattering}}(\lambda) = \frac{s(\lambda)}{a(\lambda) + s(\lambda)} \cdot (1 - e^{-(a(\lambda)+s(\lambda))\cdot L}), \text{ and} \tag{2}$$

$$P_{\text{absorption}}(\lambda) = \frac{a(\lambda)}{a(\lambda) + s(\lambda)} \cdot (1 - e^{-(a(\lambda)+s(\lambda))\cdot L}), \tag{3}$$

where $a(\lambda)$ is the absorption coefficient [11],

$$a(\lambda) = \sum_n a_i(\lambda) c_i, \tag{4}$$

$s(\lambda)$ is the reduced scattering coefficient [11],

$$s(\lambda) = s(500\,\text{nm}) \cdot \left(f_{\text{Ray}} \left(\frac{\lambda}{500\,\text{nm}} \right)^{-4} + (1 - f_{\text{Ray}}) \left(\frac{\lambda}{500\,\text{nm}} \right)^{-b_{\text{Mie}}} \right) \text{ and} \tag{5}$$

L is the length of the light path (in cm), which is assumed to be the same as the thickness of the layer. In the previous equations (4) and (5) a_i are absorption coefficients (in cm^{-1}) for each pigment, c_i are their concentrations (in fractions of total concentration), $s(500\,\text{nm})$ is the measured reduced scattering coefficient (in cm^{-1}) at 500 nm, f_{Ray} is the Rayleigh scatterings part of total scattering and b_{Mie} is Mie scattering power.

For the scattered state, the scattering and absorption probabilities are the same as for up/down states in the same layer. The up/down probabilities are

$$P_{\text{up}} = P_{\text{down}} = \frac{P_{\text{up/down}}}{2}, \tag{6}$$

as the photon can now go both ways. The probability of direct reflection is given as a parameter to the model $P_{dr} = 0.02$ and therefore transition probability to the first layers down state is $1 - P(dr) = 0.98$. Transition probabilities from absorbed, reflected or emitted state to itself is 1, and transition between states that are not connected is impossible.

The parameters needed for calculating the transition probabilities include pigment concentrations in skin layers, scattering coefficients and thicknesses of the skin layers and blood oxygenation level. These are sufficiently described in [11] and listed in Table 1. Example reflectance spectrum produced by SM can be seen in Figure 2. The values used in creating Figure 2 can be seen in Table 2.

Table 1 Input parameters and their ranges for Stochastic Model.

Input parameter	Range	Layer
Melanosome volume fraction	0 - 0.08	Epidermis
Blood volume fraction	0 - 0.01	Dermis
Blood oxygen fraction	0.2 - 0.5	Dermis
Water volume fraction	0.5 - 0.8	Dermis
Reduced scattering coefficient at 500nm (cm^{-1})	38 - 58	Both
Rayleigh scattering fraction	0.38 - 0.42	Both
Mie scattering power	0.3 - 1	Both
Thickness of epidermis (cm)	0.005 - 0.035	Epidermis
Thickness of dermis (cm)	0.1 - 0.4	Dermis

Table 2 Input parameters and their ranges for Stochastic Model and Kubelka-Munk Model in Figure 2.

Input parameter	Value for SM	Value for KM
Melanosome volume fraction	0.1	0.1
Blood volume fraction	0.02	0.02
Blood oxygen fraction	0.5	0.5
Water volume fraction	0.4	*Not applicable*
Reduced scattering coefficient at 500nm (cm^{-1})	48	48
Rayleigh scattering fraction	0.41	0.41
Mie scattering power	0.7	0.7
Thickness of epidermis	0.007 cm	0.000 07 m
Thickness of dermis	0.2 cm	0.002 m
Anisotropy	*Not applicable*	0

2.2 Kubelka-Munk Model

Kubelka-Munk Model (KM) is a special case solution to the radiative transfer equation [17]. The model consists of two differential equations for opposing light fluxes I and J:

$$\begin{cases} \frac{dI}{dx} &= -KI - SI + SJ \\ \frac{dJ}{dx} &= -KJ - SJ + SI, \end{cases} \tag{7}$$

where K and S are absorption and scattering functions, and x is the thickness of the media. Their reasoning and analytical solution can be found for example in [22].

Our implementation of the model follows the implementation described in [12]. Compared to that we changed the scattering coefficient to the same we used in SM, from [11]. The model takes into account the two first main layers of the skin: epidermis and dermis. Light that goes through these layers is considered absorbed. The parameters and their used ranges are adapted from [11, 12] and are described in Table 3. Details of the implementation can be found in [12]. Example spectrum produced by KM can be seen in Figure 2. The values used in creating Figure 2 can be seen in Table 2.

Table 3 Inputs and their ranges for KM.

Input parameter	Range	Layer
Melanosome volume fraction	0.01 - 3.01	Epidermis
Blood volume fraction	0.001 - 0.501	Dermis
Blood oxygen fraction	0.6 - 0.99	Dermis
Reduced scattering coefficient at 500nm (cm^{-1})	38 - 58	Both
Rayleigh scattering fraction	0.38 - 0.42	Both
Mie scattering power	0.3 - 1	Both
Thickness of epidermis (m)	0.0001 - 0.0006	Epidermis
Thickness of dermis (m)	0.001 - 0.004	Dermis
Anisotropy	0.7 - 0.8	Both

2.3 Convolutional neural network

Convolutional neural network (CNN) is a neural network where at least one of the traditional fully connected layers is replaced with convolutional layer [18]. It has been found useful in various tasks including image and signal type data [16, 13, 28, 5, 24].

Our CNN implementation can be seen in Table 4. It consists of two convolutional layers and three dense layers. Additionally there are two pooling layers and one dropout layer and the output layer. It is very conventional CNN. The optimization algorithm used is the Adam-algorithm [14] with meta parameters of learning rate =

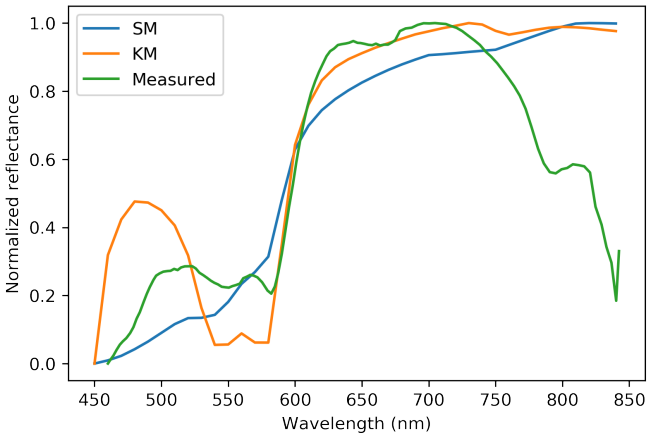

Fig. 2 Example spectra produced by stochastic and KMs using realistic values and a measured spectrum.

0.001, $\beta_1 = 0.9$, $\beta_2 = 0.999$, $\epsilon = 1 \cdot 10^{-7}$. As the loss function we use the mean square error. The CNN is implemented with Keras using Tensorflow backend [20]. CNN is used in inverting the KM and SM models.

Table 4 Convolutional neural network used in inversions.

Layer	Kernel / pool size or Activation	Output Shape	Parameters
Conv1D	(3) ReLU	(38, 64)	256
MaxPooling1D	(2)	(19, 64)	0
Conv1D	(3) ReLU	(17, 128)	24704
MaxPooling1D	(2)	(8, 128)	0
Flatten		(1024)	0
Dense	ReLU	(128)	131200
Dense	ReLU	(64)	8256
Dense	ReLU	(32)	2080
Dropout (0.25)		(32)	0
Dense		(9)	297
Total params:	166,793		
Trainable params:	166,793		
Non-trainable params:	0		

Table 5 Correlation coefficients of values retrieved from Stochastic Model.

Retrieved parameter	Correlation coefficient between estimated and real value
Melanosome	0.96
Blood volume fraction	0.87
Blood oxygen fraction	0.07
Water volume fraction	0.27
Reduced scattering coefficient at 500nm	0.57
Rayleigh scattering fraction	0.11
Mie scattering power	0.92
Thickness of epidermis	0.95
Thickness of dermis	0.96

2.4 Model Inversion

Both SM and KM are inversed by CNN and the inversion results are used to predict parameters from simulated and empirical data. For the inversion, the training and validation labels described in Tables 1 and 3 are scaled to range from 0 to 1 in order to receive best possible performance from CNN. Hence, the predictions are also in range from 0 to 1. For predictions using simulated data, correlation coefficients are calculated and analyzed. Predictions from empirical data are visually interpreted and their potential for further research is discussed.

Our empirical data consinsts of a hyperspectral image of human skin with a large nevus. Example spectrum can be seen in Figure 2.

3 Results and Discussion

3.1 Retrieval Results

The inversion results for SM were strongest at dermis and epidermis thicknesses and melanosome concentration, with correlations of 0.96, 0.95 and 0.96 respectively. The weakest correlations were in blood oxygenation, Rayleigh scattering fraction, and water volume fraction at 0.07, 0.11, and 0.27, respectively. Altogether three correlations could be considered weak, one moderate and five strong. (Figure 3, Table 5)

The results of the inversion of the KM had strongest retrieval correlations in blood oxygen fraction, blood volume fraction and thicknesses of epidermis and dermis at 0.99, 0.94, 0.94 and 0.92 respectively. The weakest correlations were in Rayleigh scattering fraction and Mie scattering power at 0.02 and 0.29, respectively. Altogether two correlations could be considered weak, two moderate and five strong.

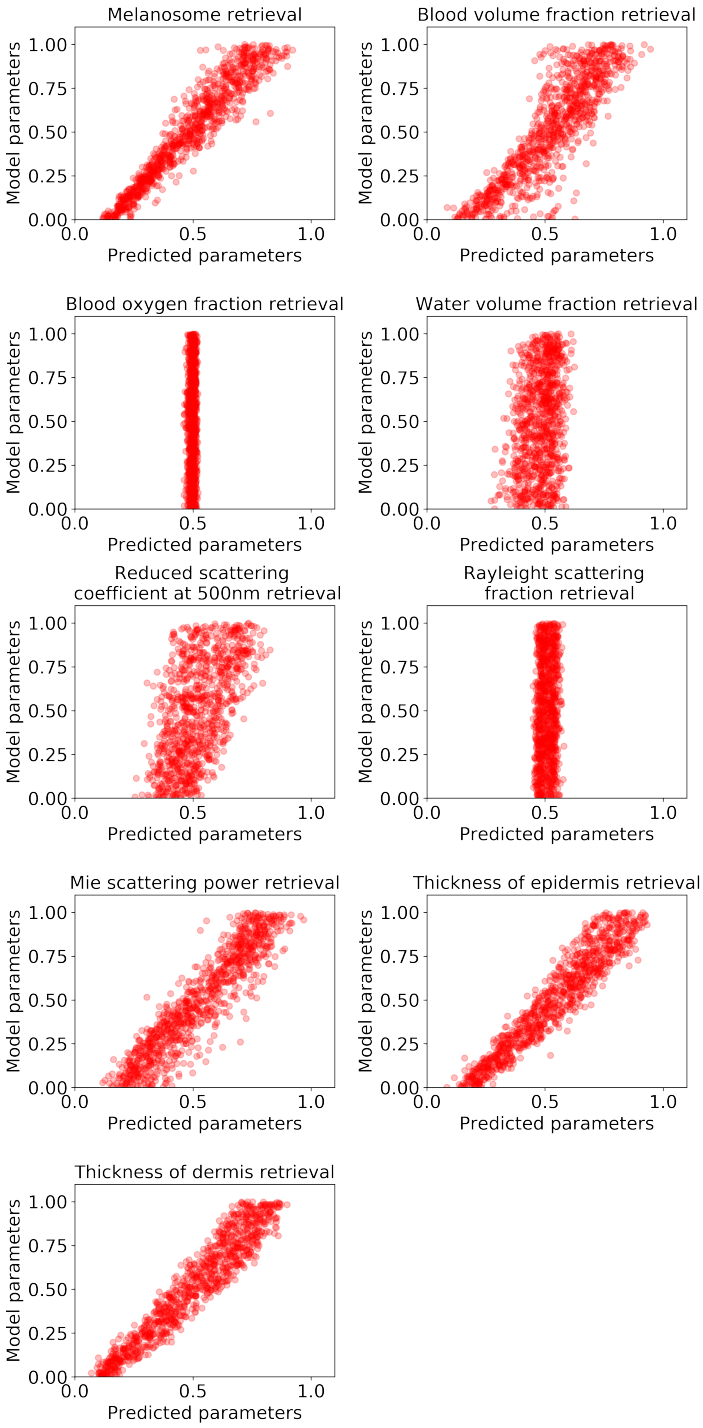

Fig. 3 Inversion of Stochastic Model.

Table 6 Correlation coefficients of values retrieved from Kubelka-Munk Model.

Retrieved parameter	Correlation coefficient between estimated and real value
Melanosome	0.89
Blood volume fraction	0.94
Blood oxygen fraction	0.99
Reduced scattering coefficient at 500nm	0.40
Rayleigh scattering fraction	0.02
Mie scattering power	0.29
Thickness of epidermis	0.94
Thickness of dermis	0.92
Anisotropy	0.39

The results for empirical data (Figure 5) showed that there is potential for further research using both models as a training data source for CNN. The models were mutually consistent in showing higher and lower values for different parameters and at least for the melanin concentration the models rightly predicted higher melanin concentrations on the area of the nevus.

3.2 Model Comparison

3.2.1 Accuracy

Both of these models seemed to produce spectra, which mimic skin reflectance, although the the effect of haemoglobin absorption (450-550 nm) in KM spectrum was suspiciously symmetrical (Figure 2). The haemoglobin absorption seems to have too much influence to the KM while the SM seems to be influenced too little. The spectrum of KM seemed similar to normal skin while the spectrum of SM appeared to be similar to pale (less blood) skin [2, 11, 15]. The fact that parameters given to the KM (Table 3) were not realistic decreases the KMs credibility. Especially melanosome volume fraction was too high. The accuracy of the KM we used has been partially verified previously by inverting the model with evolutionary algorithm and retrieving plausible pigment concentrations from living skin [12].

The accuracy of SM was verified in previous research with pigments typical to plants [19]. The modifications we made did not change the mathematical core of the model, therefore the accuracy of the model is derived from the accuracy of the pigment absorption spectrums.

The accuracy of the inversions varied for both models. From SM, predictions (Figure 3) of skin layer thicknesses and melanosome concentration were well predicted and Mie scattering power and blood volume fraction less accurately. For the rest of the parameters the accuracy was non-existent.

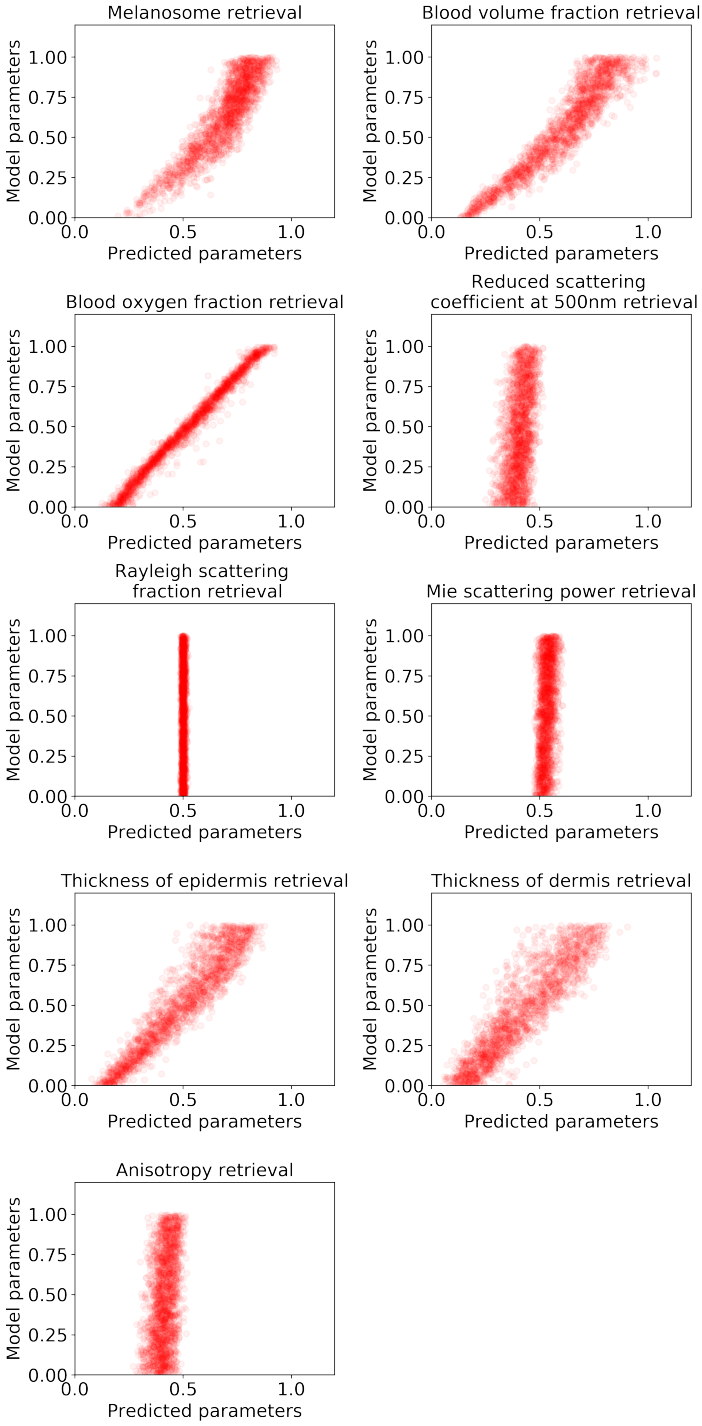

Fig. 4 Inversion of Kubelka-Munk Model.

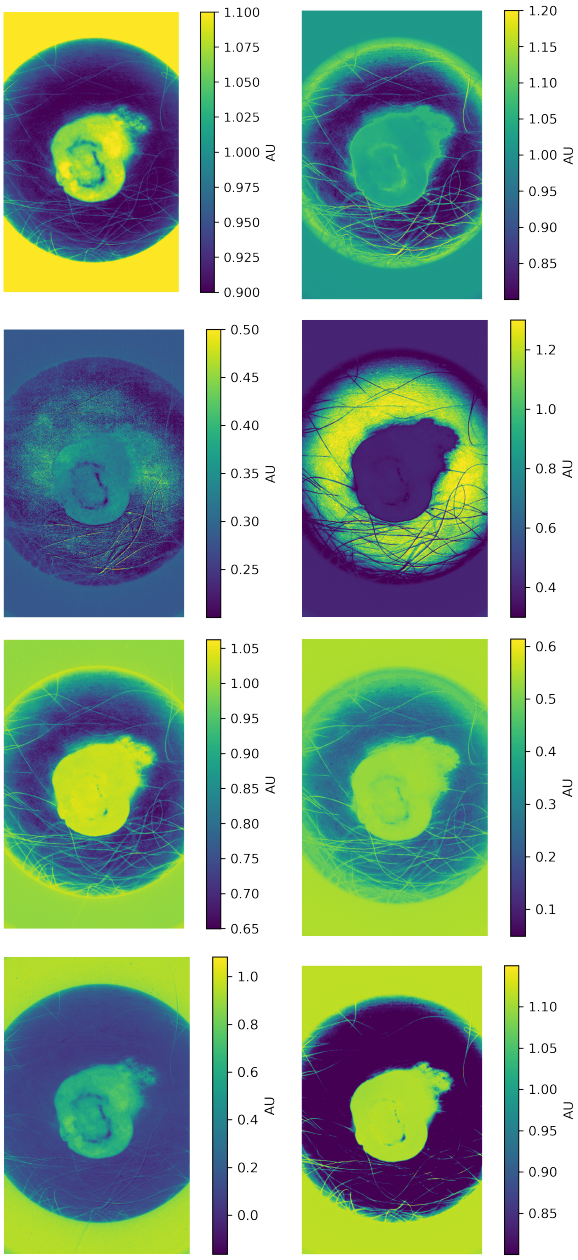

Fig. 5 Values predicted by inversed Kubelka-Munk Model (left) and Stochastic Model (right). Predicted parameters are, from top to bottom, Melanosome volume fraction, blood volume fraction, epidermis thickness and dermis thickness. The units are arbitrary.

From KM (Figure 4), the blood oxygen fraction and blood volume fraction were particularly well predicted and melanosome concentration, and skin layer thicknesses were little less accurate. Once again, for the rest of the parameters (4), the accuracy was poor.

3.2.2 Usefulness

KM is the most used in the field of colour modelling [26], and it is sufficiently accurate while being easy to understand and fast to calculate. Our implementation of SM takes a while to calculate, but it seems like it has potential to be more accurate than KM.

For physical parameter retrieval, the models were useful in different areas. For some reason the scattering parameters seemed to have little to no impact on the KM, while for the SM the result were a little bit better. KM seemed more likely to return the correct values on the actual pigment concentrations, and SM gave better results at evaluating the thicknesses of the skin layers.

3.3 Discussion

The results indicate that the both KM and SM can be used as a data augmentation source in physical parameter retrieval from skin. KMs strengths are in calculation time and its simplicity. SMs strengths are higher potential accuracy and adaptability, as the absorption and scattering coefficients are independently tunable and the layers are easily added and removed and probability calculations can be changed if needed. With more investigation the reason for the irretrievable parameters could be found. The easiest hypothesis is that they simply do not affect the spectrum enough to be retrieved, and based on Figure 2, this seems to be the case for SM. Water absorption in the studied wavelength range is quite small compared to the other parameters [11], and haemoglobin absorption has a negative peak between 450 nm and 550 nm [15], and our SM does not seem to show it. In KM retrieval, only parameters related to scattering are poorly retrieved. They are also poorly retrieved in SM and they appear to affect the spectrum very little.

When we compare the spectra in Figure 2 to previous research it is clear that the measured skin spectra can be replicated pretty closely [2]. The empirical implications are left for further research, but this research and previous research have given us reason to believe that the SM can be well adapted for accurate skin reflectance modelling [19]. If this holds, it means that we could use SM and a skin structure model to produce accurate training data for machine learning applications in medical field. This would decrease the need for data gathering for such application. However, measured data always includes noise, therefore one needs to find a way to introduce realistic noise to the model.

4 Conclusion

We have demonstrated that the Stochastic Model originally developed for leaf optical properties can be successfully transported to skin reflectance modelling by changing equations and parameters of the model to skin related equations and parameters. We have demonstrated that the model has similar accuracy with Kubelka-Munk Model, while being easier to modify. It is up for debate if the probability and transition net based Stochastic Model is easier to understand when compared to Kubelka-Munk Model, which is based on solutions of a differential equations. The most direct implications of our work are, that the model should be first verified and further adapted to skin reflectance modelling and then tested in machine learning applications in the medical field.

References

1. R. Rox Anderson and John A. Parrish. The Optics of Human Skin. *Journal of Investigative Dermatology*, 77(1):13–19, July 1981.
2. Elli Angelopoulou. Understanding the color of human skin. In *Human Vision and Electronic Imaging VI*, volume 4299, pages 243–251. International Society for Optics and Photonics, June 2001.
3. M. Gorji Bandpay, F. Ameri, K. Ansari, and S. Moradian. Mathematical and empirical evaluation of accuracy of the Kubelka–Munk model for color match prediction of opaque and translucent surface coatings. *Journal of Coatings Technology and Research*, 15(5):1117–1131, September 2018.
4. Gladimir VG Baranoski and Tenn F Chen. Multilayer modeling of skin color and translucency. 2014.
5. Hubert Cecotti and Axel Graeser. Convolutional neural network with embedded Fourier transform for EEG classification. In *Pattern Recognition, 2008. ICPR 2008. 19th International Conference on*, pages 1–4. IEEE, 2008.
6. B. L. Diffey. A mathematical model for ultraviolet optics in skin. *Physics in Medicine and Biology*, 28(6):647–657, June 1983.
7. Motonori Doi and Shoji Tominaga. Spectral estimation of human skin color using the Kubelka-Munk theory. In *Color Imaging VIII: Processing, Hardcopy, and Applications*, volume 5008, pages 221–228. International Society for Optics and Photonics, 2003.
8. John Hammersley. *Monte carlo methods*. Springer Science & Business Media, 2013.
9. Clare F Heal, Beverley A Raasch, PG Buettner, and David Weedon. Accuracy of clinical diagnosis of skin lesions. *British Journal of Dermatology*, 159(3):661–668, 2008.
10. Akira Ishimaru. *Wave propagation and scattering in random media*, volume 2. Academic press New York, 1978.
11. Steven L Jacques. Optical properties of biological tissues: a review. *Physics in Medicine & Biology*, 58(11):R37, 2013.
12. Romuald Jolivot, Yannick Benezeth, and Franck Marzani. Skin parameter map retrieval from a dedicated multispectral imaging system applied to dermatology/cosmetology. *Journal of Biomedical Imaging*, 2013:26, 2013.
13. Andrej Karpathy, George Toderici, Sanketh Shetty, Thomas Leung, Rahul Sukthankar, and Li Fei-Fei. Large-scale video classification with convolutional neural networks. In *Proceedings of the IEEE conference on Computer Vision and Pattern Recognition*, pages 1725–1732, 2014.
14. Diederik P Kingma and Jimmy Ba. Adam: A method for stochastic optimization. *arXiv preprint arXiv:1412.6980*, 2014.

15. Aravind Krishnaswamy and Gladimir VG Baranoski. A study on skin optics. *Natural Phenomena Simulation Group, School of Computer Science, University of Waterloo, Canada, Technical Report*, 1:1–17, 2004.
16. Alex Krizhevsky, Ilya Sutskever, and Geoffrey E Hinton. Imagenet classification with deep convolutional neural networks. In *Advances in neural information processing systems*, pages 1097–1105, 2012.
17. Paul Kubelka. Ein Beitrag zur Optik der Farbanstriche (Contribution to the optic of paint). *Zeitschrift fur technische Physik*, 12:593–601, 1931.
18. Yann LeCun and Yoshua Bengio. Convolutional networks for images, speech, and time-series. *The handbook of brain theory and neural networks*, 1995.
19. S. W. Maier, W. Lüdeker, and K. P. Günther. SLOP: A Revised Version of the Stochastic Model for Leaf Optical Properties. *Remote Sensing of Environment*, 68(3):273 – 280, 1999.
20. Martín Abadi, Ashish Agarwal, Paul Barham, Eugene Brevdo, Zhifeng Chen, Craig Citro, Greg S. Corrado, Andy Davis, Jeffrey Dean, Matthieu Devin, Sanjay Ghemawat, Ian Goodfellow, Andrew Harp, Geoffrey Irving, Michael Isard, Yangqing Jia, Rafal Jozefowicz, Lukasz Kaiser, Manjunath Kudlur, Josh Levenberg, Dandelion Mané, Rajat Monga, Sherry Moore, Derek Murray, Chris Olah, Mike Schuster, Jonathon Shlens, Benoit Steiner, Ilya Sutskever, Kunal Talwar, Paul Tucker, Vincent Vanhoucke, Vijay Vasudevan, Fernanda Viégas, Oriol Vinyals, Pete Warden, Martin Wattenberg, Martin Wicke, Yuan Yu, and Xiaoqiang Zheng. *TensorFlow: Large-Scale Machine Learning on Heterogeneous Systems*. 2015.
21. Noora Neittaanmäki, Mari Salmivuori, Ilkka Pölönen, L Jeskanen, A Ranki, O Saksela, E Snellman, and M Grönroos. Hyperspectral imaging in detecting dermal invasion in lentigo maligna melanoma. *British Journal of Dermatology*, 177, 2017.
22. James H. Nobbs. Kubelka—Munk Theory and the Prediction of Reflectance. *Review of Progress in Coloration and Related Topics*, 15(1):66–75, 1985.
23. Ilkka Pölönen, Samuli Rahkonen, Leevi Annala, and Noora Neittaanmäki. Convolutional neural networks in skin cancer detection using spatial and spectral domain. In *Photonics in Dermatology and Plastic Surgery 2019*, volume 10851, page 108510B. International Society for Optics and Photonics, 2019.
24. Justin Salamon and Juan Pablo Bello. Deep convolutional neural networks and data augmentation for environmental sound classification. *IEEE Signal Processing Letters*, 24(3):279–283, 2017.
25. Mari Salmivuori, N Neittaanmäki, Ilkka Pölönen, L Jeskanen, Erna Snellman, and Mari Grönroos. Hyperspectral imaging system in the delineation of Ill-defined basal cell carcinomas: a pilot study. *Journal of the European Academy of Dermatology and Venereology*, 33(1):71–78, 2019.
26. T. Shakespeare. *Colorant modelling for on-line paper coloring: evaluations of models and an extension to Kubelka-Munk model*. Number 304 in Tampereen teknillinen korkeakoulu. Julkaisuja. Tampere University of Technology, 2000.
27. M Shimada, Y Yamada, M Itoh, and T Yatagai. Melanin and blood concentration in a human skin model studied by multiple regression analysis: assessment by Monte Carlo simulation. *Physics in Medicine & Biology*, 46(9):2397, 2001.
28. Christian Szegedy, Alexander Toshev, and Dumitru Erhan. Deep neural networks for object detection. In *Advances in neural information processing systems*, pages 2553–2561, 2013.
29. Martin JC Van Gemert, Ashley J Welch, Willem M Star, Massoud Motamedi, and Wai-Fung Cheong. Tissue optics for a slab geometry in the diffusion approximation. *Lasers in medical Science*, 2(4):295–302, 1987.
30. Saurabh Vyas, Jon Meyerle, and Philippe Burlina. Non-invasive estimation of skin thickness from hyperspectral imaging and validation using echography. *Computers in biology and medicine*, 57:173–181, 2015.
31. San Wan, R Rox Anderson, and John A Parrish. Analytical modeling for the optical properties of the skin with in vitro and in vivo applications. *Photochemistry and Photobiology*, 34(4):493–499, 1981.

32. Lihong Wang, Steven L Jacques, and Liqiong Zheng. MCML—Monte Carlo modeling of light transport in multi-layered tissues. *Computer methods and programs in biomedicine*, 47(2):131–146, 1995.